Mon. Not. R. Astron. Soc. **000**, 1–13 (2004) Printed 2 February 2008 (MN LATEX style file v2.2)

Bias in the Estimation of Global Luminosity Functions

O. Ilbert[1⋆], L. Tresse[1], S. Arnouts[1], E. Zucca[2], S. Bardelli[2], G. Zamorani[2], C. Adami[1], A. Cappi[2], B. Garilli[4], O. Le Fèvre[1], D. Maccagni[4], B. Meneux[1], R. Scaramella[5], M. Scodeggio[4], G. Vettolani[3], A. Zanichelli[3]
[1] *Laboratoire d'Astrophysique de Marseille, Les Trois-Lucs, B.P. 8, 13376, Marseille Cedex 12, France*
[2] *INAF, Osservatorio Astronomico di Bologna, via Ranzani 1, 40127 Bologna, Italy*
[3] *Istituto di Radioastronomia-CNR, via Gobetti 101, 40129 Bologna, Italy*
[4] *Istituto di Astrofisica Spaziale e Fisica Cosmica del CNR, via Bassini 15, 20133 Milano, Italy*
[5] *Ossevatorio Astronomico di Roma, Via Ossevatorio 2, 00040 Monteporzio Carone (Roma), Italy*

Accepted. Received; in original form

ABSTRACT

We discuss a bias present in the calculation of the global luminosity function (LF) which occurs when analysing faint galaxy samples. This effect exists because of the different spectral energy distributions of galaxies, which are in turn quantified by the k-corrections. We demonstrate that this bias occurs because not all galaxy types are visible in the same absolute magnitude range at a given redshift and it mainly arises at high redshift since it is related to large k-corrections. We use realistic simulations with observed LFs to investigate the amplitude of the bias. We also compare our results to the global LFs derived from Hubble Deep Field-North and -South (HDF) surveys. We conclude that, as expected, there is no bias in the global LF measured in the absolute magnitude range where all galaxy types are observable. Beyond this range the faint-end slope of the global LF can be over/under-estimated depending on the adopted LF estimator. The effect is larger when the reference filter in which the global LF is measured, is far from the rest-frame filter in which galaxies are selected. The fact that LF estimators are differently affected by this bias implies that the bias is minimal when the different LF estimators give measurements consistent with one another at the faint-end. For instance, we show that the estimators are discrepant in the same way both in the simulated and HDF LFs. This suggests that the HDF LFs are affected by the presently studied bias. The best solution to avoid this bias is to derive the global LF in the reference filter closest to the rest-frame selection filter.

Key words: surveys - galaxies: luminosity function - galaxies: estimator

1 INTRODUCTION

The luminosity function (LF) is a fundamental and basic tool to understand and constrain the history of galaxy formation and evolution. Moreover, the derived mean luminosity density at different redshifts allows to derive estimates of the cosmic star formation density. In the distant Universe, LFs are measured in several redshift bins in order to quantify the evolution of galaxy populations. In this paper, we focus on the reliability of the statistical estimators usually used to measure the global LF. We call *global LF* the sum of the LFs per galaxy type (Binggeli et al. 1988). Calculating LFs is not a trivial task since estimators must account for all biases or limits introduced by the observational selection effects. Most of the surveys are limited in apparent magnitude. This effect is accounted for in the $1/V_{max}$ LF estimator (Schmidt 1968). The drawback of the $1/V_{max}$ method is the implicit assumption, in its formulation, of a uniform galaxy distribution (i.e. no significant over- or under-densities of galaxies). Nevertheless, because of its simplicity, this method is the most often used in high-redshift surveys. Lynden-Bell (1971) developed the C^- method to overcome the assumption of a uniform galaxy distribution. The STY (Sandage, Tammann & Yahil 1979) and the Step Wise Maximum-Likelihood LF estimators, hereafter SWML, (Efstathiou, Ellis & Peterson 1988, EEP) are both related to maximum-likelihood statistical methods. The C^-, STY and SWML methods make no assumptions on spatial distribution of galaxies, but the information about the normalization of the LF is lost. Davis & Huchra (1982) reviewed

⋆ E-mail: Olivier.Ilbert@oamp.fr

various estimators to derive the normalization. In contrast to C^- and SWML, the STY method does assume a parametric form to the luminosity distribution.

All LF estimators present both advantages and drawbacks. Willmer (1997) and Takeuchi, Yoshikawa & Ishii (2000) compared several LF estimators using simulated catalogues. Their mock catalogues did not tackle into detail the effects of k-corrections and of the mix of individual and different LF shapes for different morphological types in the measurement of the global LF. The Canada-France Redshift Survey (CFRS; Lilly et al. 1995) demonstrated that the evolution of the LF depends strongly on the studied galaxy population. In this paper we add the dependency of limiting absolute magnitudes on galaxy type in simulated catalogues, and at the same time we introduce an evolution of the LF per galaxy population to produce realistic simulations. These improvements enable us to identify an intrinsic bias in the estimators to measure the global LF.

The different visibility limits for the various galaxy types (mainly due to different k-corrections) affects all flux-limited surveys. Hence it can have an impact on statistical analyses, in particular the LF estimates. The accepted idea is that certain galaxy types sometimes can not be visible in a given redshift bin, so that it would obviously underestimate the global LF. However even though all galaxy types are visible in a given redshift bin, we show using realistic simulations that a bias still arises in the measurement of the global LF. As noted by Lilly et al. (1995), it occurs because different galaxy types are not visible in the same absolute magnitude range. In the literature this bias has never been quantified. We use real and simulated data to investigate the amplitude and the behavior of this bias. In particular our analysis is focused on high-redshift data since the k-correction values are small at low redshift.

One possible solution to avoid this bias would be to sum the extrapolated LFs per galaxy type to measure the global LF. Unfortunately this solution is hazardous in the highest redshift bins of a deep survey for two reasons: the number of galaxies is often too small to derive LFs per galaxy type and not all the LF slopes per galaxy type are well constrained, which would imply a dangerous extrapolation. The analysis of the global high-redshift LFs has been the framework of most of the previous analyses on deep surveys like, for instance, the Subaru Deep Field (SDF; Kashikawa et al. 2003), the Hubble Deep Fields (HDF; e.g. for example Sawicki, Lin & Yee 1997, Takeuchi et al. 2000, Bolzonella, Pelló & Maccagni 2002), the CFRS (Lilly et al. 1995). With the on-going or earlier deep surveys, one needs to quantify in details this bias related to k-correction effects.

This paper is organized as follows. Section 2 describes the origin of the bias linked to the spectral energy distribution dependency of absolute magnitudes. Section 3 reviews briefly the following estimators, $1/V_{max}$, STY, SWML and C^+, and the bias linked to each of them. Section 4 quantifies the impact of the bias on the global LF from simulations and from the Hubble Deep Field surveys. Section 5 presents our conclusion. Throughout this paper, we adopt an Einstein-de Sitter universe ($\Omega_0 = 1$, $\Omega_\Lambda = 0$) and $H_0 = 100$ km s^{-1} Mpc^{-1}, but the results here discussed are not dependent on the adopted cosmological model.

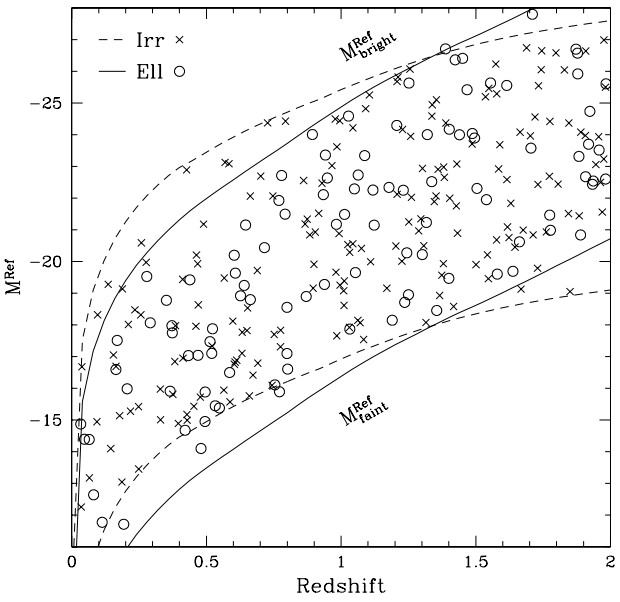

Figure 1. Example of the observable $M-z$ plane in a flux-limited survey for elliptical-type SEDs (open circles) limited by the solid lines, and irregular-type SEDs (crosses) limited by the dashed lines. Each type of galaxies is observable between its respective limits of absolute magnitudes, M^{Ref}_{bright} and M^{Ref}_{faint}. The $M-z$ planes for different SEDs do not coincide. In this example the selection filter is the I band and the absolute magnitudes are computed in the U band.

2 ORIGIN OF THE BIAS

In any flux-limited survey, galaxy i is observed within a fixed apparent magnitude range, $m^S_{bright} \leqslant m^S_i \leqslant m^S_{faint}$, where S designates the band where galaxies are selected. We use Ref to designate the reference filter corresponding to the wavelength at which the LF is estimated. The observational limits imply that galaxy i with spectral energy distribution SED_i is observable within a fixed redshift range and a fixed absolute magnitude range.

Obviously, the redshift and absolute magnitude limits depend on SED_i (see Fig. 1). That is, galaxy SED_i with absolute magnitude, M^{Ref}_i, is observable in the redshift range:

$$z_{bright}(M^{Ref}_i, \mathrm{SED}_i) \leqslant z_i \leqslant z_{faint}(M^{Ref}_i, \mathrm{SED}_i).$$

Similary galaxy SED_i at redshift z_i is observable in the absolute magnitude range:

$$M^{Ref}_{bright}(z_i, \mathrm{SED}_i) \leqslant M^{Ref}_i \leqslant M^{Ref}_{faint}(z_i, \mathrm{SED}_i).$$

The latter limits of absolute magnitudes are defined by,

$$\begin{aligned} M^{Ref}_{bright}(z, \mathrm{SED}_i) &= m^S_{bright} - DM(z) - KC(z, \mathrm{SED}_i), \\ M^{Ref}_{faint}(z, \mathrm{SED}_i) &= m^S_{faint} - DM(z) - KC(z, \mathrm{SED}_i), \end{aligned}$$

where $DM(z)$ is the distance modulus and KC is expressed as follows:

$$KC(z, \mathrm{SED}_i) = (k^{Ref}(z) + m^S(z) - m^{Ref}(z))^{\mathrm{SED}_i},$$

where k is the k-correction, and m is the apparent magnitude measured from the SED. We note that, for typical galaxy k-corrections, M^{Ref}_{bright} and M^{Ref}_{faint} are overall strictly

decreasing (i.e. increasing in brightness) as a function of redshift. Thus, in a given redshift interval, $z_{low} \leqslant z < z_{high}$, it is impossible to observe galaxy SED$_i$ fainter than $M^{Ref}_{faint}(z_{low}, \mathrm{SED}_i)$ and brighter than $M^{Ref}_{bright}(z_{high}, \mathrm{SED}_i)$. Then, in a given absolute magnitude interval, some SEDs may not be observable while others are detected. This leads to a bias intrinsic to the global LF estimated in a given redshift interval, $z_{low} \leqslant z < z_{high}$, as we describe in details in Section 3. We discuss in this paper the bias in the luminosity function induced by different SEDs. However a similar bias arises when using a magnitude limited sample to derive estimates of other distribution functions, like masses or sizes.

Of course, no bias would be present if the entire population under study had the same or very similar SEDs, as in the case of the estimate of the LF for a single galaxy type. When this is not the case, as for example in the case of galaxies of all types (from very blue to very red) an obvious bias is arising. As shown in Fig. 2, there are three possible cases, which are defined on the basis of z, λ^S (effective wavelength of the selection filter) and λ^{Ref} (effective wavelength of the reference filter):

- $1 + z_{low} < \lambda^S/\lambda^{Ref}$, the faint limiting absolute magnitude is brighter for blue galaxies than for red galaxies and therefore faint blue galaxies are missing from the sample;
- $1 + z_{low} \sim \lambda^S/\lambda^{Ref}$, the faint limiting absolute magnitude is about the same for all galaxies;
- $1 + z_{low} > \lambda^S/\lambda^{Ref}$, the faint limiting absolute magnitude is brighter for red galaxies than for blue galaxies and therefore faint red galaxies are missing from the sample.

The impact of the bias on each LF estimator depends on the case in which the analysis of the global LF is performed and on the different slopes and normalizations of red and blue galaxies. One possible way to cope with this effect is to derive the global LF in an absolute magnitude range in which all types are observable as done in e.g. Small, Sargent & Hamilton (1997). However this means to throw away from the analysis some fraction of the data. Another way is to define the sample to be analysed in such a way that $1 + z_{low} \sim \lambda^S/\lambda^{Ref}$ for each redshift bin (see e.g. Poli et al. 2001, 2003). This requires the availability of a multi-color survey, if one wants to estimate the LF in a fixed λ^{Ref} over a wide redshift range.

Fig. 2 shows the faint observable absolute magnitude limits, M^{Ref}_{faint}, as a function of z for three SEDs (E, Sp, Irr) in the case of an I-selection filter, $m^I_{faint} = 26$ mag. In Fig. 2, three reference filters are considered: UV(2000 Å), B(4500 Å) and I(8140 Å). For illustration purposes, we consider galaxy populations in the redshift range $0.70 \leqslant z_i < 1.25$. Let us consider the case of the UV reference filter (top panel of Fig. 2). Irregular-type SEDs are visible in the whole z interval $[0.70, 1.25]$ if they are brighter than $M^{UV} = -16.0$ (case a). They are still visible, but not in the whole z interval, if $-16.0 < M^{UV} < -14.2$ (case b). Finally, irregular-type SEDs fainter than $M^{UV} = -14.2$ mag are not visible at all in this z interval (case c). In case a, no correction for missing objects has to be applied when computing the LF. In case b, LF estimators enable to correct for the fact that some galaxies cannot be visible in the whole redshift range. In case c, the global LF cannot be measured because irregular-type SEDs are lost. The same considerations apply

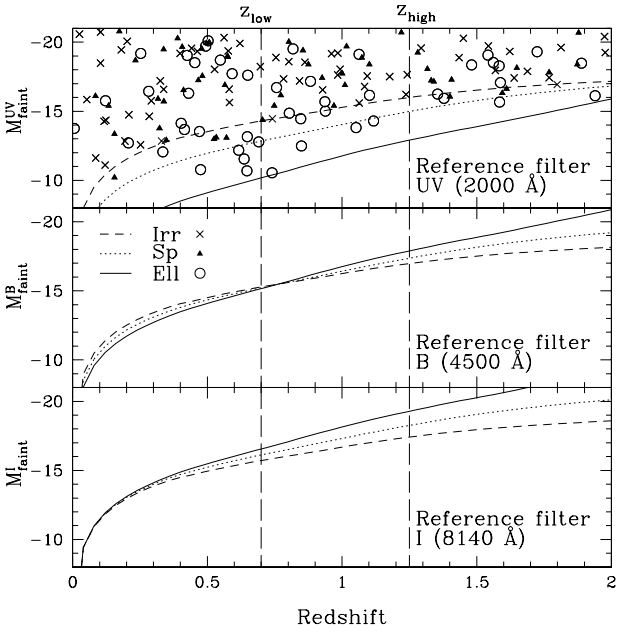

Figure 2. Faint observable absolute magnitude limits in different reference filters as a function of redshift for various SEDs (see Section 2). The filter to select galaxies is I with $I_{AB} \leqslant 26$ mag. The reference filters are respectively the UV FOCA filter (2000 Å), the B HST filter (4500 Å), the I HST filter (8140 Å). In each panel, we show three templates from a set of SEDs described in Section 4.1; solid, dotted and short-dashed lines represent elliptical-, spiral- and irregular-type SED galaxies respectively. Vertical long dashed lines define the studied redshift interval, $0.7 \leqslant z < 1.25$. In the top panel, we illustrate positions of observable galaxies with open circles for elliptical-type SEDs, filled triangles for spiral-type SEDs, and crosses for irregular-type SEDs.

for spiral- and elliptical-type SEDs, except that the observable M^{UV} limits have different values. In our first example (UV reference filter), faint galaxies of the irregular-type SEDs become unobservable in an absolute magnitude range where galaxies with other SEDs can still be detected. The resulting estimate of the global LF would start to be biased, because of the absence from the sample of these galaxies, for absolute magnitude bins fainter than $M^{UV} = -14.2$. As shown in the top panel of Fig. 2, in this example the luminosity function for elliptical type SEDs can be estimated down to $M^{UV} \sim -10.0$. As a consequence, the range of magnitudes over which the estimate of the global LF would be biased is of the order of 4 magnitudes. Obviously, this range is much smaller and close to zero when the rest frame wavelength corresponding to the selection filter is close to the reference filter (see, for example, the middle panel in Fig. 2, where Ref = B). In case Ref = I, the biased range spans about one magnitude (bottom panel of Fig. 2), but in this case are the early type SEDs which are missing from the sample in an absolute magnitude range where irregular type SEDs are still visible.

In summary, the bias we are discussing arises when estimating the LFs of the entire galaxy population in deep surveys because of the dependency of limiting absolute magnitudes on galaxy types. In estimating LFs, particular care has to be taken in the faintest absolute magnitude bins, where

some SEDs are no longer observable, thus introducing a bias in the measurement of the LFs. There is no bias in a the absolute magnitude range where all SEDs can be observed. In the case where the redshift bin starts at $z_{low} = 0$, the bias does not appear since all SEDs have the same faintest observable absolute magnitude limit.

3 BIAS INTRINSIC TO THE LUMINOSITY FUNCTION ESTIMATORS

In this section, we describe the intrinsic bias which arises when one applies the commonly used LF estimators, $1/\mathrm{V_{max}}$, $\mathrm{C^+}$, SWML and STY to estimate the global LF of the population composed by objects with different SEDs. We here describe the case of a magnitude limited sample with both bright and faint apparent magnitude cuts, m^S_{bright} and m^S_{faint}. In a given redshift interval, $[z_{low},\ z_{high}]$, the minimum and maximum observable redshifts for galaxy i are $z_{min,i} = \max[z_{low},\ z_{bright}(M_i^{Ref}, \mathrm{SED}_i)]$ and $z_{max,i} = \min[z_{high},\ z_{faint}(M_i^{Ref}, \mathrm{SED}_i)]$. We call N_g, the total number of galaxies observed in the redshift interval, $z_{low} \leqslant z < z_{high}$. We first analyse the $1/\mathrm{V_{max}}$ and $\mathrm{C^+}$ estimators which are biased in a similar way with respect to the measurement of the global LF; then we analyse the maximum-likelihood methods, SWML and STY.

3.1 The $1/\mathrm{V_{max}}$ and $\mathrm{C^+}$ estimators

3.1.1 The $1/V_{\max}$ estimator

The maximum observable comoving volume in which galaxy i can be detected, is given by

$$V_{obs,i} = \int_{\omega}\int_{z_{min,i}}^{z_{max,i}} \frac{d^2V}{d\omega dz} d\omega dz, \quad (1)$$

where ω is the effective solid angle of the survey, and V is the comoving volume. The LF measured in the reference filter Ref, $\phi^{Ref}(M)$, is discretized in bins of absolute magnitudes with width dM as follows:

$$\phi^{Ref}(M) = \sum_{k=1}^{N_{bin}} \phi_k^{Ref} W(M_k^{Ref} - M), \quad (2)$$

where the window function W is defined as,

$$W(M_k^{Ref} - M) = \begin{cases} 1 & \text{if } -dM/2 \leqslant M_k^{Ref} - M < dM/2 \\ 0 & \text{otherwise,} \end{cases} \quad (3)$$

and the discrete values of the LF, ϕ_k^{Ref}, are derived in each absolute magnitude bin k as follows:

$$\phi_k^{Ref} dM = \frac{1}{V_{total}} \sum_{i=1}^{N_g} \frac{V_{total}}{V_{obs,i}} W(M_k^{Ref} - M_i^{Ref}), \quad (4)$$

where V_{total} is the comoving volume between z_{low} and z_{high}. Although not necessary, the term V_{total} is introduced to point out the weight, $\frac{V_{total}}{V_{obs,i}}$, applied to each galaxy i. Galaxies which belong to the non observable redshift range, $[z_{low},\ z_{min,i}] \cup [z_{max,i},\ z_{high}]$, contribute to ϕ_k^{Ref} through this weight. This weighting scheme assumes a homogenous galaxy distribution, and it enables the estimator to recover the right number of galaxies with the same SED_i in the redshift bin.

3.1.2 The C^+ estimator

Lynden-Bell (1971) derived the $\mathrm{C^-}$ method. We use a modified version of the $\mathrm{C^-}$, called $\mathrm{C^+}$ (Zucca et al. 1997). The contribution of each galaxy i to the LF in the reference filter, Ref, can be expressed by the following recursive expression:

$$\psi(M_i^{Ref}) = \frac{1 - \sum_{j=1}^{i-1} \psi(M_j^{Ref})}{C^+(M_i^{Ref})}, \quad (5)$$

where galaxies are sorted from the faintest ($j = 1$) to the brightest absolute magnitude, and $\mathrm{C^+}$ is the number of galaxies with $M^{Ref} < M_i^{Ref}$ and $z_{low} \leqslant z < z_{max,i}$. The cumulative luminosity function in Eq. 5 is normalized to unity at the minimum luminosity of the galaxies in the sample. The absolute normalization A is then derived using the method described in EEP88.

The LF in a given absolute magnitude bin k is then the sum of the contributions of all galaxies to this bin,

$$\phi_k^{Ref} dM = A \sum_{i=1}^{N_g} \psi(M_i^{Ref}) W(M_k^{Ref} - M_i^{Ref}). \quad (6)$$

$\psi(M_i^{Ref})$ is the contribution of galaxy i to ϕ_k^{Ref}, and this contribution enables to recover the right number of galaxies with the same SED_i in the redshift bin.

3.1.3 Intrinsic bias in the global $1/V_{\max}$ and C^+ LFs

Let us consider the k^{th} bin of the LF, of width dM, centered on M_k^{Ref}. Let us take the following example, $M_{faint}^{Ref}(z_{low}, \mathrm{SED}_1) = M_k^{Ref} - dM/2$ and $M_{faint}^{Ref}(z_{low}, \mathrm{SED}_2) < M_k^{Ref} + dM/2$. In this case, both SEDs are observed in bin $(k-1)$. SED_1 and SED_2 galaxies contribute separately to ϕ_{k-1}^{Ref}, and thus ϕ_{k-1}^{Ref} is well recovered. In bin k, SED_1 galaxies are no more observable and only SED_2 galaxies contribute to ϕ_k^{Ref}. As a consequence, ϕ_k^{Ref} is equal to the LF of SED_2 galaxies. In Fig. 3 we show the bias of the global LF estimated with the $1/\mathrm{V_{max}}$ method (open circles) and with the $\mathrm{C^+}$ method (open squares), adopting different input LFs for the two SEDs. In the upper-panel, we adopt the same LF for the SED_1 late-type and SED_2 early-type galaxies. In the lower-panel, different slopes have been used for the input LFs ($\alpha = -1.6$ for late types and $\alpha = -0.5$ for early types). In both cases, beyond the absolute magnitude limit where late-type SEDs are not observable, the $1/\mathrm{V_{max}}$ and the $\mathrm{C^+}$ methods recover the slope of the remaining galaxy population. An other way to explain the bias which affects the $1/\mathrm{V_{max}}$ and $\mathrm{C^+}$ estimators is the following. If we derive the individual LFs of SED_1 and SED_2, the estimators recover properly the LFs per type. The absolute magnitude ranges in which the two LFs are estimated are not the same; summing these LFs per type without extrapolating at fainter absolute magnitudes the LF derived for SED_1 late-type galaxies is exactly the same thing as directly deriving the global LF for the $1/\mathrm{V_{max}}$ and $\mathrm{C^+}$ estimators. It clearly appears that in the absolute magnitude range $[-17.7, -13.5]$ we are summing the LF of the remaining type (SED_2). In the case of a number of galaxies large enough to derive LF per type, one possible solution to overcome the bias would be to derive the global LF by summing the extrapolated LFs per type. We note that the $\mathrm{C^+}$ normalization (using EEP88 method) is slightly overestimated. We

have checked that this normalization method recovers the input normalization only if the LF is estimated with SWML or STY methods, and not with the C^+ method.

In conclusion, the $1/V_{max}$ and C^+ methods lead always to underestimating the LF in the faintest absolute magnitude bins, thus biasing the global faint-end slope of the LF.

3.2 The maximum likelihood estimators

3.2.1 The STY and SWML estimators

The STY (Sandage et al. 1979) and the SWML (e.g. EEP88) estimators are both derived from maximum-likelihood methods. The likelihood $\mathcal{L}$ is the probability to obtain a sample equal to the observed one within the apparent magnitude limits of the survey. $\mathcal{L}$ is computed as the product of the probabilities to observe each galaxy at M_i^{Ref},

$$\mathcal{L} = \prod_{i=1}^{N_g} p(M_i^{Ref}) = \prod_{i=1}^{N_g} \frac{\phi^{Ref}(M_i^{Ref})}{\int_{M_{bright}^{Ref}(z_i,\mathrm{SED}_i)}^{M_{faint}^{Ref}(z_i,\mathrm{SED}_i)} \phi^{Ref}(M) dM}, \quad (7)$$

where $M_{faint}^{Ref}(z_i, \mathrm{SED}_i)$ and $M_{bright}^{Ref}(z_i, \mathrm{SED}_i)$ are the faint and bright observable absolute magnitude limits of galaxy i at z_i (see Section 2). We maximize $\mathcal{L}$ with respect to the LF. For the STY estimator, a functional form for the LF is assumed. We use the Schechter function (Schechter 1976). For the SWML estimator, the LF is discretized into absolute magnitude bins (see Eq. 2). No assumption is made about the LF shape. The STY parametric and SWML non-parametric estimators are complementary. The error bars in the SWML estimator are derived from the covariance matrix and the normalization is the sum of the inverse of the selection function of each galaxy as described in EEP88.

3.2.2 Intrinsic bias in the global SWML and STY LFs

The SWML and STY estimators are biased in a different way with respect to the $1/V_{max}$ and C^+ estimators. Let us write $\mathcal{L}$ as the product of $\mathcal{L}_1$ and $\mathcal{L}_2$, which are respectively the likelihood for SED_1 and SED_2 galaxy populations within a given redshift interval where their faintest observable absolute magnitudes are $M_{faint}^{Ref}(z_{low}, \mathrm{SED}_1) < M_{faint}^{Ref}(z_{low}, \mathrm{SED}_2)$. The global LF is well recovered in the absolute magnitude range $]-\infty, M_{faint}^{Ref}(z_{low}, \mathrm{SED}_1)]$ where both SEDs are observable. For $M_{faint}^{Ref}(z_{low}, \mathrm{SED}_1) < M_i^{Ref} \leqslant M_{faint}^{Ref}(z_{low}, \mathrm{SED}_2)$, the shape of the LF is only constrained by the probability of SED_2 population, since SED_1 population is not detected in this range of absolute magnitudes. Thus the global LF has the same shape as the SED_2 LF. In the range $]M_{faint}^{Ref}(z_{low}, \mathrm{SED}_1), +\infty[$, the SWML and STY methods estimate the shape of the SED_2 LF rather than the shape of the global LF. Three cases may occur as follows. First, the LF of SED_1 and SED_2 populations have the same shape; the global LF is well recovered. Second, the SED_2 LF has a flatter faint-end slope; the global LF is underestimated. Third, the SED_2 LF has a steeper faint-end slope than SED_1; the global LF is overestimated. The first two cases are illustrated in Fig. 3. In the bottom panel of Fig. 3, the estimate of the LF derived with the SWML method does not follow a Schechter function. Thus, the STY estimate, which assumes a Schechter parametric function and which has the same behavior as a SWML method, is not able to recover the input.

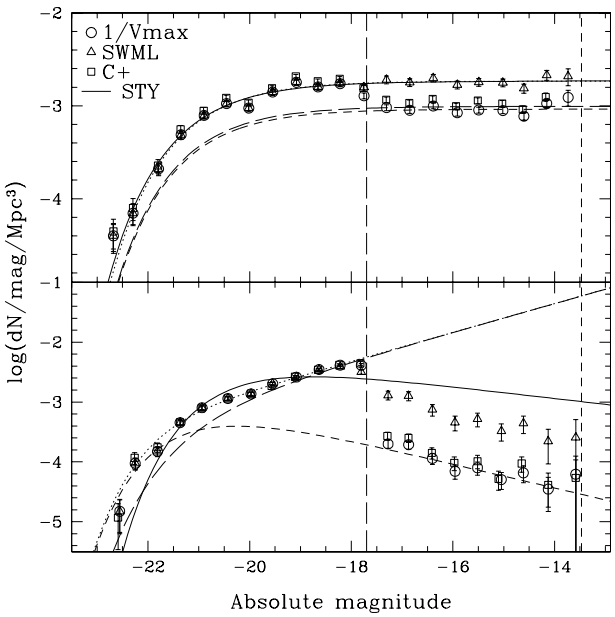

Figure 3. We simulate a simple mock catalogue with two SEDs of galaxies. SED_1 late-type galaxy population has a faint observable absolute magnitude limit at -17.7 mag (long-dashed vertical line) and an input LF shown by the long-dashed curved line. SED_2 early-type galaxy population has a fainter observable limit at -13.5 mag (short-dashed vertical line) and an input LF shown by the short-dashed curved line. The input global simulated LF is the dotted curved line, which is the sum of the input LFs of SED_1 and SED2. In the top panel, the input LFs for SED_1 and SED_2 are the same. The $1/V_{max}$ LF estimate (circles) and the C^+ LF estimate (squares) do not recover the input global LF at magnitudes fainter than -17.7 mag where SED_1 is no more observable, and thus the estimate is equal to the SED_2 LF. The SWML LF estimate (triangles) and the STY estimate (solid line) recover the input global LF since their shapes are constrained by the shape of SED_2 input LF only, which is the same as SED_1 input LF. In the bottom panel, the input LFs for SED_1 and SED_2 have a faint-end slope $\alpha = -1.6$ and $\alpha = -0.5$ respectively. At magnitudes fainter than -17.7 mag, where SED_1 population is no more detected, the $1/V_{max}$ LF and the C^+ LF are equal to SED_2 input LF. The SWML and STY LF faint-ends (constrained by the shape of SED_2 input LF) are underestimated.

In conclusion, the bias in the faint-end slope of the global LF estimated with likelihood methods depends on the LF shape of each SED. Thus to quantify the bias, we need to use simulations which deal with LF per SED, as we do below.

4 APPLICATIONS TO SIMULATED AND REAL DATA

In this section, we give a description of the Hubble Deep Field (HDF) data and simulations (Section 4.1), then we illustrate the bias in a qualitative way using the HDF data (Section 4.2), and finally we quantify the bias with 1,000

Spectral class	$\Phi^* \times 10^{-3}\mathrm{Mpc}^{-3}$	α	M_R^*
Early	14.77	0.11	−20.56
Spiral	13.61	−0.73	−20.43
Irr	6.52	−1.64	−19.84

Table 1. Input LF parameters per spectral class in the R band (in Vega system) used for the simulations in Section 4.

simulations of the HDF survey and the Virmos-VLT Deep Survey (VVDS) (Section 4.3).

4.1 Brief description of the data

We use the public version of the multi-color mock catalogues from Arnouts (2004) available at *www.lam.oamp.fr/arnouts/LE_PHARE.html*. Simulations are based on an empirical approach using observed LFs to derive redshift and apparent magnitude distributions. The LFs of the ESO-Sculptor Survey (ESS; de Lapparent et al. 2003) are implemented up to redshift $z < 0.6$ for early, spiral and irregular spectral types (see Tab. 1). The LF evolution per type beyond $z \sim 0.6$ is constrained in a way that it reproduces the observed redshift, number count and color distributions. We made the following assumptions as in Arnouts (2004): the LFs of early and spiral class are constant with redshift; the faint-end slope for the three LFs is constant; for the irregular class there is an evolution in density in the redshift range $0.15 < z \leqslant 0.7$ using $\phi^*(z) = \phi^*(1 + 3.69(z - 0.15))$, and an evolution in luminosity in the redshift range $1.25 < z \leqslant 2.5$ using $M^*(z) = M^* - 0.12(z - 1.25)$. Mock catalogues are derived using the set of SEDs as described in Arnouts et al. (1999), composed of 72 SEDs that have been interpolated between four observed spectra of Coleman et al. (1980) and two starburst models, computed with GISSEL (Bruzual & Charlot 1993). The set of SEDs is divided into three main spectral classes: elliptical, spiral and irregular galaxies. Since a spectral class corresponds to several different SEDs, the bias may arise also within a single class. To test this last point, we also use only one SED per spectral class, even though the simulation with a set of only three SEDs is less realistic.

We used the photometric catalogue and the photometric redshifts of the HDF South and North surveys from Arnouts et al. (1999, 2002). Our aim is to illustrate the bias with observational data, and it is not to derive the best LF of the HDF. The HDF survey is taken as an example of a survey in which, because of the relatively small number of observed galaxies, only the global LF, rather than the LF for different galaxy types, can be reliably derived in different redshift bins. For consistency in the comparison, the HDF data have been analysed using exactly the same set of 72 SEDs as in the simulation.

4.2 Qualitative description of the bias

We describe the bias using HDF data and one simulation from which data have been selected with the same apparent magnitude limits as the HDF data. To illlustrate the bias in a qualitative way, we use a large number of galaxies ($> 5,000$ in each redshift bin) so that statistical uncertainties become negligible. Moreover we did not include any surface brightness effect and any uncertainties on apparent magnitudes, redshifts, and absolute magnitudes. We derived the absolute magnitudes and the global LFs in two redshift intervals: $0.70 \leqslant z < 1.25$ and $1.25 \leqslant z < 2.00$ in the following reference filters, UV (Fig. 4a), B (Fig. 4b) and I (Fig. 4c) with samples selected at $I_{AB} \leqslant 26$ mag. In these figures, we plot the input LFs of the simulation (one for each spectral type and the global one) and the estimates of the global LF derived by the $1/\mathrm{V_{max}}$, C^+, SWML and STY methods from mock catalogues and the HDF data. Before discussing in detail each figure, we note that in all cases the estimators give similar results using the mock catalogues constructed with three SEDs only and those with 72 SEDs. We display the simulations with three SEDs so to compare exactly to the three input simulated LFs per class (i.e. per SED in this case). With 72 SEDs such a comparison is less obvious since each class contains several SEDs. However we show also the simulations with 72 SEDs so it is comparable to the analysis applied to the HDF data, that is with the same selection function, the same set of SEDs and the same filters.

4.2.1 UV-rest LFs

In the left panels of Fig. 4a, we show the individual input LFs (dotted lines) of the mock catalogue built with three SEDs, that is with one SED per spectral class. The sum of the three individual input LFs corresponds to the global simulated LF (solid line). Thus the LF estimators should be able to recover this global LF in estimating the LF for the whole galaxy sample. First, we note that all estimators underestimate the faint-end of the LFs. As previously shown in Fig. 2, the irregular-type galaxies 'disappear' from the faintest absolute magnitude bins (for $M^{UV} > -14.2$ mag at $z_{low} = 0.7$ and $M^{UV} > -16.0$ mag at $z_{low} = 1.25$). As explained in Section 3 when one type 'disappears' the global LF estimate is based only on the remaining types.

Left panels of Fig. 4a show this point; the $1/\mathrm{V_{max}}$ and C^+ estimators recover the input LF of elliptical galaxies in the faintest absolute magnitude bins (i.e. open circles and squares overlap the dotted line of the elliptical-type LF). The SWML method underestimates the faint-end slope of the global LF since this estimator recovers the shape of the elliptical-type galaxies (i.e. open triangles follow the same slope as the elliptical-type LF). The less biased result is obtained with the STY method and the more biased results are obtained with the $1/\mathrm{V_{max}}$ and C^+ methods. It is interesting to note in the redshift interval $1.25 \leqslant z < 2.0$ that the little 'bump' of the global SWML LF estimate at $M^{UV} \sim -15$ mag corresponds to the shape the elliptical-type input LF.

In the middle panels, we show the global LF derived using the mock catalogue with 72 SEDs distributed into three spectral classes. We see that the increase of the number of SEDs used per spectral class does not affect significantly the trend of the LF estimators described above. Using many SEDs smooths the effect of the 'disappearance' of a SED.

In the right panels, we show the global LF derived from the HDF data using the same 72 SEDs as in the mock catalogue. We do not observe very faint (and very bright) galaxies as observed in the simulation even though both data sets

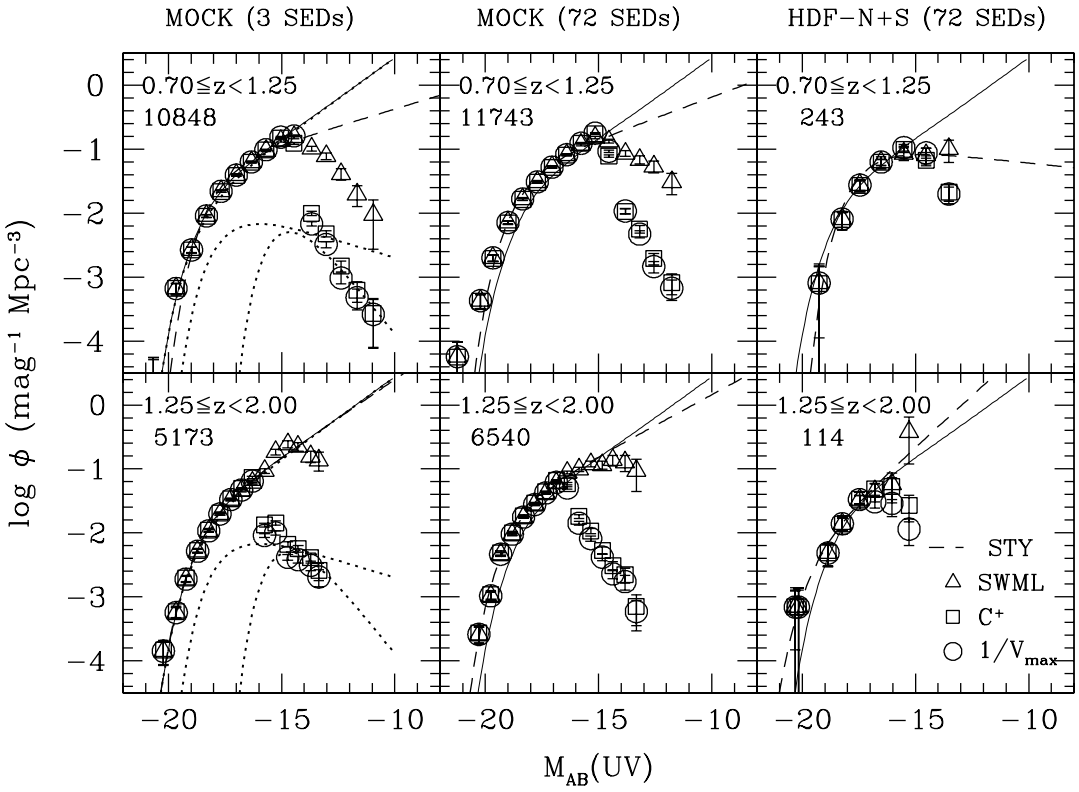

Figure 4.a Global luminosity functions derived in the UV-FOCA (2000 Å) reference filter in two redshift intervals, $0.70 \leqslant z < 1.25$ (top panels), $1.25 \leqslant z < 2.0$ (bottom panels). The left and middle panels correspond to the LFs derived from simulations with 3 and 72 SEDs respectively. The right panels correspond to the LFs derived from the HDF-North and -South surveys. The limiting magnitude in all cases is $I_{AB}(8140\ \text{Å}) < 26$ mag. In the left panels, we display the LFs corresponding to the three input SEDs used (dotted lines): from the steepest to the shallowest slope, it is the irregular-, spiral- and elliptical-type LF respectively. In each panel, we plot the global simulated LF (solid line) corresponding to the sum of the three input LFs. We plot also the results from the following global LF estimates, STY (dashed line), SWML (triangles), C^+ (squares), and $1/V_{max}$ (circles). Below the z redshift intervals we quote the number of galaxies used to derive the LFs. We adopt Poissonian error bars for the $1/V_{max}$ and C^+ estimators. The error bars for the SWML estimator are derived following the EEP88 method.

have the same selection function. We have tested that this is indeed due to the relatively small number of galaxies observed in the HDF and the small probability to observe the faintest (and brightest) galaxies. Thus, the difference between the various estimators is less obvious than in the simulation. However we note here the same general trend in the faintest observed bins. This may suggest that the bias which affects the global HDF LF estimation is similar to the bias shown in the simulation. In conclusion the faint-end of the global LF cannot be properly recovered by any estimator as can be seen from the comparison with the global simulated LF (solid line).

4.2.2 B-rest LFs

We plot in Fig.4b the global LF in the B reference filter with the same symbols as in Fig.4a. The simulations built with both three and 72 SEDs give exactly the same result. At $z = 0.7$, the B-filter absolute magnitudes are almost independent on SEDs since the selection filter (I) roughly corresponds to the B-rest filter at this redshift. As a consequence, all

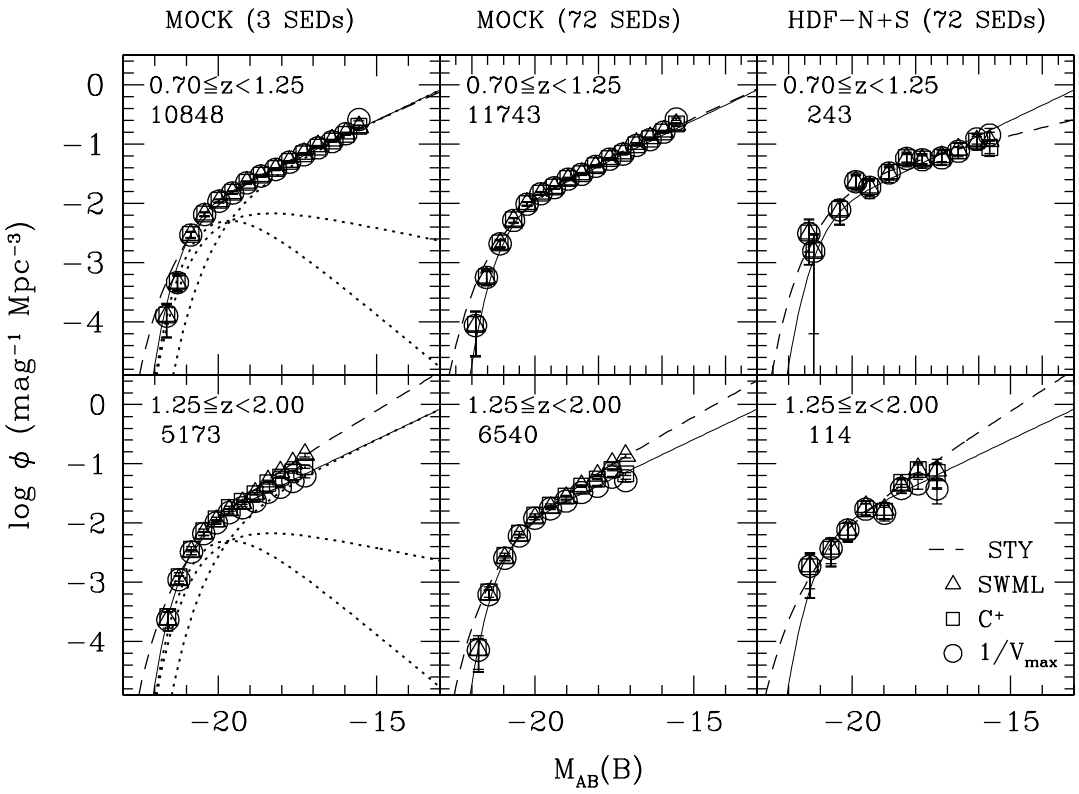

Figure 4.b Same as Fig. 4a except that the reference filter is B-HST (4500 Å).

estimators recover very well the global simulated LF in the first redshift bin ($0.70 \leqslant z < 1.25$). For the HDF data, the four estimators are in agreement amongst them. The bias is not present in this case, as shown by our simulation.

In the redshift bin $1.25 \leqslant z < 2$, the SWML and the STY methods slightly overestimate the slope of the global LF. At $z_{low} = 1.25$, the limiting absolute magnitude M^B_{faint} for early types is about one magnitude brighter than for late types. Thus the SWML and STY estimators measure the steep slope of the late-type galaxies, and this explains the overestimate of the faint-end slope of the global measured LF. The $1/V_{max}$ and C^+ methods well recover the global simulated LF, since the density of the first type which 'disappears' from the sample (that is the faint elliptical-type galaxies) is negligible in the global simulated LF. Global LF estimators from the HDF data are globally in agreement amongst them. The estimate of the global LF in the B reference filter is quite robust.

4.2.3 I-rest LFs

For the I-rest LFs, the range of absolute magnitudes in which different spectral types 'disappear', increases with redshift since the reference filter is also the filter used to select the sample. At $z = 0.7$, this range spans one magnitude (see Fig. 2), thus all estimators should be slightly biased in the redshift bin $0.7 \leqslant z < 1.25$. We note that all LF estimators recover the global simulated LF in simulations derived with three as well as with 72 SEDs. For the HDF LF, the estimators are in good agreement with each other and this suggests that the measurement is not biased.

At $z = 1.25$, the absolute magnitude range in which different spectral types 'disappear' spans more than two magnitudes. In this case the first spectral types which 'disappear' from the faintest bins are the elliptical types. In both simulations, the SWML and STY methods largely overestimate the slope of the faint-end in the redshift bin $1.25 \leqslant z < 2.00$, while the $1/V_{max}$ and C^+ methods recover reasonably well

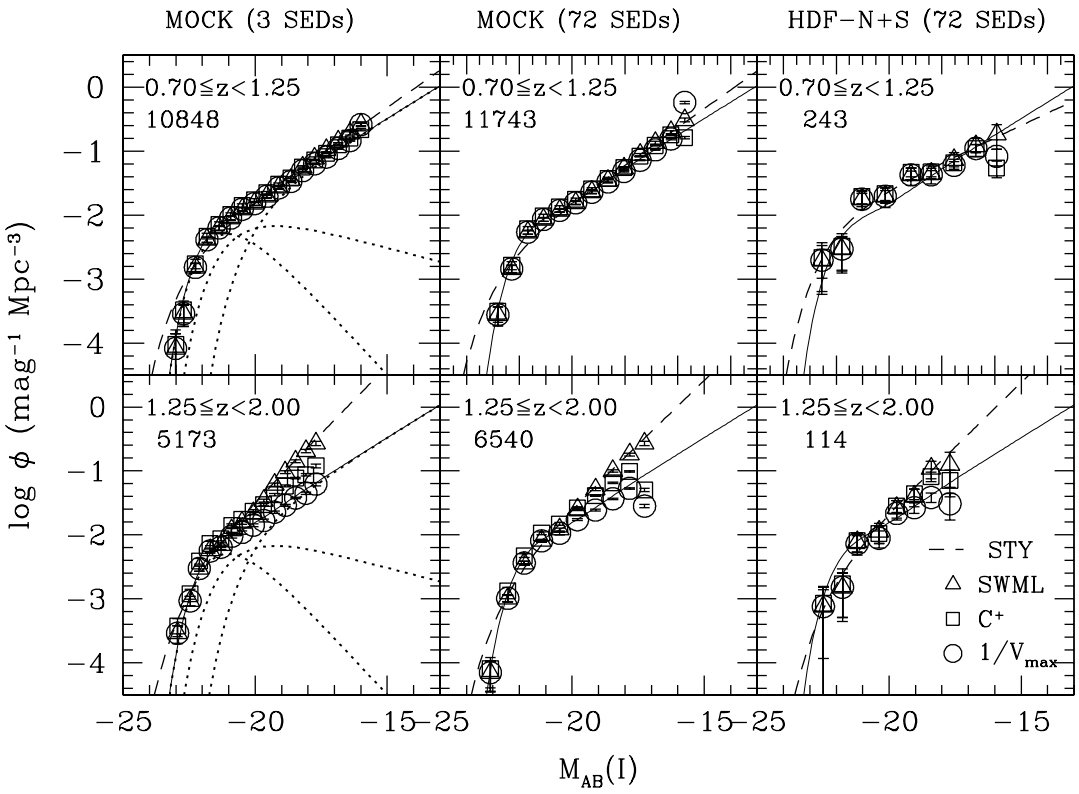

Figure 4.c Same as Fig. 4a except that the reference filter is I-HST (8140 Å).

(the $1/V_{max}$ method better than the C^+ method) the faint-end of the global LF. Indeed, the slope estimated with the SWML and STY methods is the slope of the irregular galaxies, which is steeper than the global input LF slope in the range of absolute magnitudes here measured. The $1/V_{max}$ and C^+ estimators recover the slope of the global LF since the contribution of the faint elliptical-type galaxies to the global LF is negligible. In the global LF derived from the HDF data, the SWML and STY estimators predict a steeper slope than the $1/V_{max}$ and C^+ estimators, as in the simulations. According to the simulations, the global LF derived from the HDF data and estimated with the SWML and STY overestimate the faint-end slope in the redshift bin $1.25 \leqslant z < 2.00$.

4.3 Quantitative measurement of the bias

As shown throughout the paper, the bias depends on the band in which galaxies are selected, on the apparent limits of the survey, on the reference band in which the LF is measured, and on the lower limit of a studied redshift bin. Thus we cannot provide here a recipe to quantify the amplitude of the bias in all cases. We choose to quantify it in the following specific cases, the HDF and the Virmos-VLT Deep Survey (VVDS) surveys. The HDF is a good example where we can derive the global LF only. The VVDS is a deep spectroscopic survey with enough galaxies to derive the LFs per type (Le Fèvre 2004). The global LF is also a necessary output of the VVDS survey, however even in this case, deriving it from the sum of extrapolated LFs per type may be dangerous. We produced 1,000 simulations representative of HDF and VVDS surveys. Realistic apparent magnitude errors are introduced in each simulation, and this has resultant uncertainties on the template fit, k-corrections and absolute magnitudes. We do not include any surface brighness effects and errors on the redshift.

We choose the Schechter parameters to quantify the bias. The parameter α is the most affected by the bias. In

consequence, we fix M^* for the LF estimation of each simulations. We call $\Delta\alpha$, the difference between the estimated α value and the input α value to the simulations and $\overline{\Delta\alpha}$ the average value of $\Delta\alpha$ over 1,000 realizations.

In the simulations, we have implemented LFs per type. Then to compare the estimates of the global LF with the input, we had to define a 'pseudo' input global LF. We did that in the following way.

- We realize one big simulation with more than 1,000 galaxies in each redshift bin so to minimize statistical fluctuations.
- We do not include any errors on redshifts, apparent magnitudes, absolute magnitudes, and types.
- To obtain a global LF which is not affected by the bias in the big simulation, we select galaxy samples three magnitudes fainter than the apparent magnitude limits of the 1,000 simulations representative of HDF and VVDS. And then the absolute magnitude range is limited to the same absolute magnitude range spanned by the LF estimates of these 1,000 realizations. The Schechter parameters are derived with the STY method.

4.3.1 Bias quantified for HDF

Each simulation of the HDF is realized on 8 arcmin^2 and with $I_{AB} \leqslant 26$. The LFs are derived in three reference bands (UV-FOCA, B-HST and I-HST) and in four redshift bins from $z = 0.5$ to $z = 2$. The results of these simulations are shown in Fig. 5.

In the UV (2000 Å) band (first column of the figure), the estimate of the faint-end slope with the $1/V_{max}$ fit is strongly underestimated ($\overline{\Delta\alpha} > 0.5$ for $z \geqslant 0.75$), while the STY estimate is only slightly biased ($\overline{\Delta\alpha} \simeq 0.1$). In the B-HST band (second column), the LF estimates derived with the STY and the $1/V_{max}$ methods are robust up to the redshift bin [1, 1.5]. In the redshift bin [1.5, 2], the STY estimate gives ~ -0.30 steeper values for the α parameter, whereas the $1/V_{max}$ fit gives ~ 0.20 flatter values. In the I band (third column), the bias from the STY estimate increases as a function of redshift; the input α parameter is recovered in the first redshift bin, and $\overline{\Delta\alpha}$ decreases down to -0.40 in the last redshift bin [1.5, 2]. The $1/V_{max}$ fit gives an estimate which recovers the input α up to the reshift bin [1, 1.5].

4.3.2 Bias quantified for VVDS

We quantify now the amplitude of the bias for a sample selected in a way similar to the VVDS. We adopt the Johnson Kron-Cousins filter set and we perform each simulation on 360 arcmin^2. The sample selected from each simulation is approximatively of the same size ($\sim 7,000$ galaxies) as the presently available spectroscopic deep sample in the 0226-0430 VVDS field. The global LF estimations are derived in three reference bands, U (3600 Å), B (4200 Å) and I (8000 Å), and in four redshift bins from $z = 0.6$ to $z = 1.5$. For our illustration, we consider two cases of sample selection; an I-selected sample (as the VVDS spectroscopic data), and an U-selected sample (as for instance, a VVDS photometric data).

The results of these simulations are shown in the Fig. 6. We show in the first column the U-band LF estimates for samples selected in the U band with $U_{AB} \leqslant 24$. The bias increases with redshift. In all redshift bins, the STY estimate gives steeper faint-end slopes ($\overline{\Delta\alpha} \sim -0.3$), and the $1/V_{max}$ fit gives flatter faint-end slopes ($\overline{\Delta\alpha} > 1$ for $z \geqslant 1$).

In the second column, samples are selected with $I_{AB} \leqslant 24$, and the LF estimates are derived in the U band. Like for the HDF, the faint-end slope is underestimated by both the STY method and the $1/V_{max}$ fit in the first redshift bin ($\overline{\Delta\alpha} \sim 0.2$ and $\overline{\Delta\alpha} \sim 0.5$ respectively). The bias decreases with redshift. In the last redshift bin, all estimates recover the input α value because the rest-frame selection I-band corresponds to the reference U-band at $z \sim 1.2$.

In the third column, samples are selected with $I_{AB} \leqslant 24$, and the LF estimates are derived in the reference B-band. The input α parameter is recovered by both methods up to $z = 1$. The STY estimation of α in the redshift bin [1, 1.2] is only slightly biased ($\overline{\Delta\alpha} \sim -0.1$), while it is strongly biased in the last redshift bin [1.2, 1.5]. The STY estimate gives steeper faint-end slopes ($\overline{\Delta\alpha} \sim -0.4$), and the $1/V_{max}$ fit gives flatter faint-end slopes ($\overline{\Delta\alpha} \sim 0.2$).

In the last column, samples are selected with $I_{AB} \leqslant 24$, and the LF estimates are derived in the reference I-band. The bias increases with redshift. The $1/V_{max}$ fit gives flatter faint-end slopes (up to $\overline{\delta\alpha} \sim 0.4$ for $1.2 \leqslant z < 1.5$). The STY estimate gives steeper faint-end slopes (up to $\overline{\Delta\alpha} \sim -1$ for $1.2 \leqslant z < 1.5$).

In conclusion, in deep surveys like the HDF or the VVDS, the various estimators fail to correctly recover the global LF faint end if the reference filter is far from the rest-frame selection filter. If the results from different estimators are not in good agreement with each other, the global LF estimate is likely to be biased and the only way to quantitatively estimate this bias is through a detailed comparison with simulations representing to the sample properties.

5 CONCLUSIONS

Our study enabled us to describe when LF estimators are robust for the measurement of the global LF in the framework of the earlier and future deepest surveys. We demonstrated that the estimation of the global LF contains an intrinsic bias due to the fact that, in a magnitude limited sample, different galaxy types have different limits in absolute magnitude because of different k-corrections. The importance of the effect is larger when the range of k-correction between the different galaxy types is wide. For this reason this bias mainly arises in high redshift samples. The STY and SWML estimators are not affected in the same way by this bias as the $1/V_{max}$ and C^+ estimators. If the STY, SWML and the $1/V_{max}$, C^+ methods are not in good agreement with each other, this is an indication that the bias in the global LF estimators is present. A good indication of the presence of a significant bias is when the differences between different estimators (Vmax and STY for instance) is larger than the statistical uncertainties (Poisson errors for instance). We quantified it using realistic simulations and observations for galaxies selected in the I filter, and measuring the LF in various reference filters (UV, B, I). We obtain the following results.

(i) Case $1 + z_{low} < \lambda^S/\lambda^{Ref}$ (e.g., a reference-frame UV

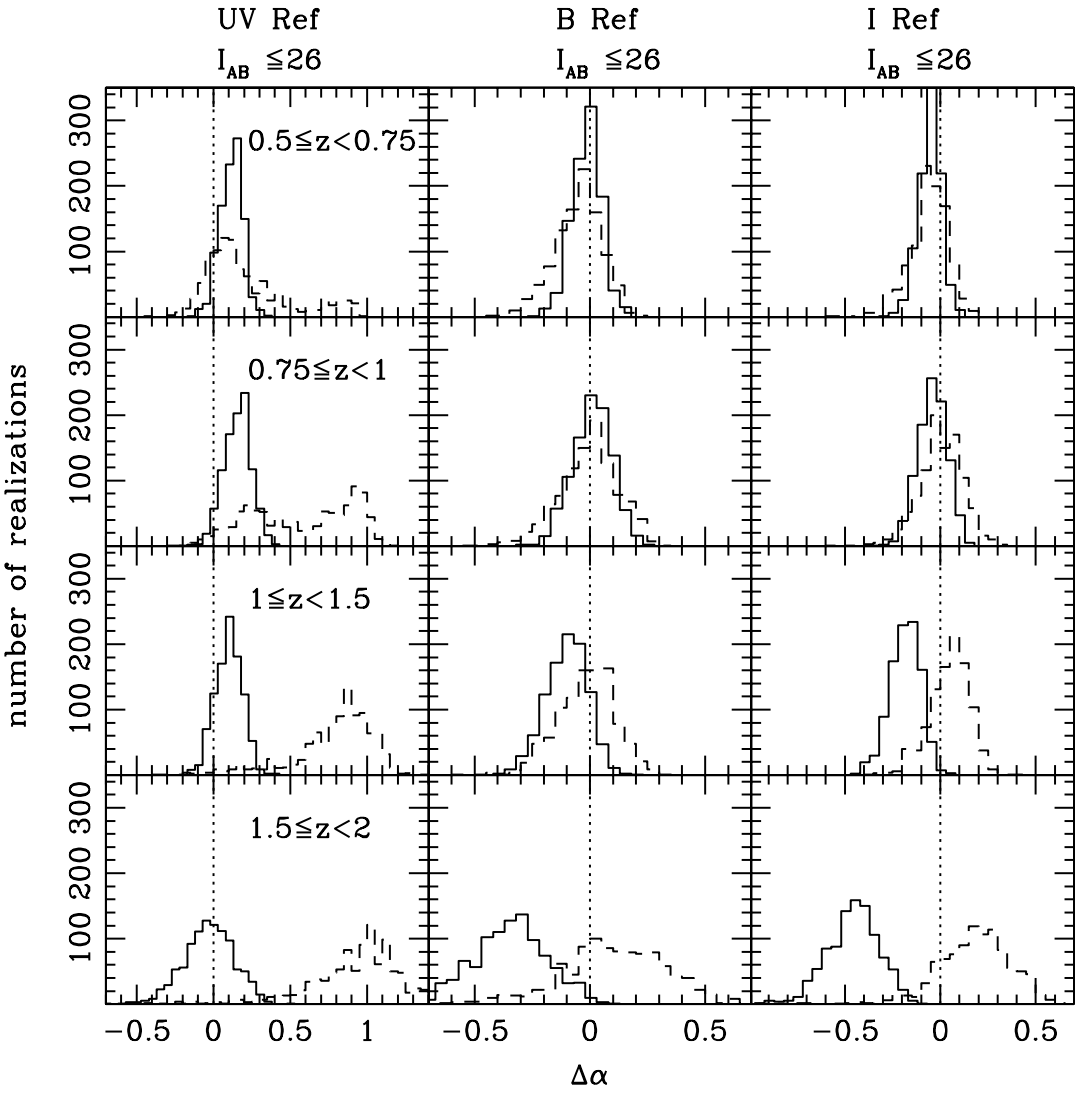

Figure 5. Histograms of the differences, $\Delta\alpha$, between the estimated and the input α parameters, over 1,000 realizations done with the HDF characteristics. $\Delta\alpha$ for the STY estimates is the solid line histogram, while $\Delta\alpha$ for the $1/V_{max}$ fit is the dashed-line histogram. All the simulated HDF samples are selected with $I_{AB} \leqslant 26$. Panels in the first column correspond to the case with the global LFs derived in the UV-FOCA (2000 Å) filter, in the middle column in the B-HST (4500 Å) filter, and in the right column in the I-HST (8140 Å) filter. From top to bottom panels, $\Delta\alpha$ is measured within the redshift bins [0.5, 0.75], [0.75, 1], [1, 1.5], [1.5, 2].

LF for galaxies selected in I): the studied estimators underestimate the faint-end slope of the global LF for $z_{low} \lesssim 2$. This underestimate is particulary significant for the $1/V_{max}$ and C^+ methods (i.e. for instance, the UV-LF of the SDF).
(ii) Case $1 + z_{low} \sim \lambda^S/\lambda^{Ref}$ (e.g., a reference-frame B LF for galaxies selected in I): the estimators of the global LF are robust up to $z_{low} \lesssim 1.3$. In this redshift range the bias is minimal (i.e. for instance, the CFRS case).
(iii) Case $1 + z_{low} > \lambda^S/\lambda^{Ref}$ (e.g., a reference-frame I LFs with galaxies selected in I): the STY and SWML methods overestimate the faint-end slope of the global LF, while the $1/V_{max}$ method roughly recovers well the global LF (e.g., for instance, the redshift bin [1.25, 2] of the HDF).

The ways to reduce the intrinsic bias of the global LF estimators are the following:

(a) The selection of galaxy subsamples in the closest rest-frame filter to the reference filter in which the LF is measured (see e.g. Poli et al. 2001, 2003). This method is also the best to reduce the SED dependency in the measurement of absolute magnitudes since in this case the term [color+k-correction] is little dependent on the SED. Only multi-color surveys allow to derive the same rest-frame band LF at different redshifts using this strategy.

(b) In principle, the estimate of the global LF using the sum of the extrapolated LF per galaxy type. However it requires a good knowledge of the slope for all the LFs per type, and in practice the use of extrapolated LFs may be hazardous.

(c) The estimate of the global LF using a filter in which the differences between k-corrections are small, as for instance

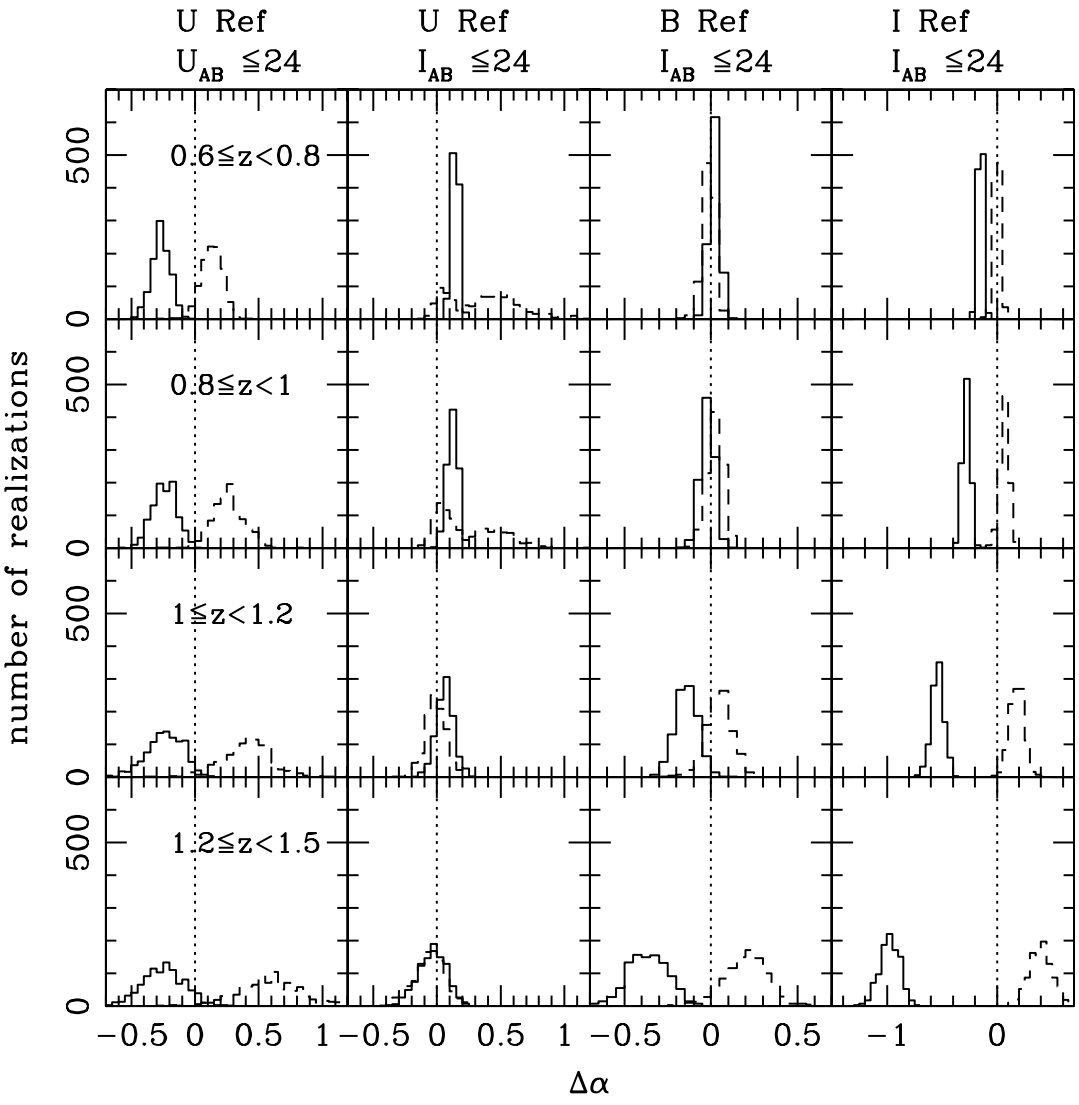

Figure 6. Same as in Fig. 5 except that the simulations are selected in a way similar to the VVDS. Panels in the first column correspond to samples selected with $U_{AB} \leqslant 24$, and the other columns correspond to samples selected with $I_{AB} \leqslant 24$. In the first and second column, the global LFs are derived in the U (3600 Å) reference filter, the third column in the B (4300 Å), and the last column in the I (8000 Å). From top to bottom panels, $\Delta\alpha$ is measured within the redshift bins [0.6, 0.8], [0.8, 1], [1, 1.2], [1.2, 1.5].

in the K-filter, e.g. Bolzonella et al. (2002), Pozzetti et al. (2003).

(d) The estimate of the global LF within an absolute magnitude range in which all galaxy types are detected (see e.g. Small et al. 1997). This method is appropriate for very large surveys like the VVDS for instance, at the cost of the loss of the faintest bins of the global LF.

ACKNOWLEDGMENTS

This work has been developed within the framework of the VVDS Consortium. We thank the referee for the careful reading of the manuscript and the useful suggestions.

REFERENCES

Arnouts S., Cristiani S., Moscardini L., Matarrese S., Lucchin F., Fontana A., Giallongo E., 1999, MNRAS, 310, 540

Arnouts S. et al., 2002, MNRAS, 329, 355

Arnouts S. et al., 2004, in preparation

Binggeli B., Sandage A., Tammann G. A., 1988, ARA&A, 26, 509

Bolzonella M., Pelló R., Maccagni D., 2002, A&A, 395, 443

Bruzual A. G., Charlot S., 1993, ApJ, 405, 538

Coleman G. D., Wu C.-C., Weedman D. W., 1980, ApJS, 43, 393

Davis M., Huchra J., 1982, ApJ, 254, 437

De Lapparent V., Galaz G., Bardelli S., Arnouts S., 2003, A&A, 404, 831

Efstathiou G., Ellis R. S., Peterson B. A., 1988, MNRAS, 232, 431 (EEP)
Kashikawa N. et al., 2003, AJ, 125, 53
Le Fèvre O. et al., 2004, in preparation
Lilly S. J., Tresse L., Hammer F., Crampton D., Le Fèvre O., 1995, ApJ, 455, 108
Lynden-Bell D., 1971, MNRAS, 155, 95
Poli F., Menci N., Giallongo E., Fontana A., Cristiani S., D'Odorico S., 2001, ApJ, 551, L45
Poli F. et al. 2003, ApJ, 593, L1
Pozzetti, L. et al., 2003, A&A, 402, 837
Takeuchi T. T., Yoshikawa K., Ishii T. T., 2000, ApJS, 129, 1
Sandage A., Tammann G. A., Yahil A., 1979, ApJ, 232, 352
Sawicki M. J., Lin H., Yee H. K. C., 1997, AJ, 113, 1
Schechter P., 1976, ApJ, 203, 297
Schmidt M., 1968, ApJ, 151, 393
Small T. A., Sargent W. L. W., Hamilton D., 1997, ApJ, 487, 512
Steidel C. C., Adelberger K. L., Giavalisco M., Dickinson M., Pettini M., 1999, ApJ, 519, 1
Willmer C. N. A., 1997, AJ, 114, 898
Zucca E. et al., 1997, A&A, 326, 477